SYSTEM OPTIMIZTION OF HOT WATER CONCENTRATED SOLAR THERMOELECTRIC GENERATION

Kazuaki Yazawa and Ali Shakouri

University of California Santa Cruz; USA

Abstract

In this report, we describe the design of a concentrated solar thermoelectric (TE) system which can provide both electricity and hot water. Today's thermoelectric materials have a relatively low efficiency (~6% for temperature difference across the thermoelement on the order of 300°C). However since thermoelectrics don't need their cold side to be near room temperature, (in another word, one can chose the particular thermoelectric material to match to the operational temperature) it is possible to use the waste heat to provide hot water and this makes the overall efficiency of the combined system to be quite high. A key factor in the optimization of the thermoelectric module is the thermal impedance matching with the incident solar radiation, and also with the hot water heat exchanger on the cold side of the thermoelectric module. We have developed an analytic model for the whole system and optimized each component in order to minimize the material cost. TE element fill factor is found to be an important parameter to optimize at low solar concentrations (<50) in order to obtain the highest amount of electric power generated per mass of the thermoelectric elements. Similarly the co-optimization of the microchannel heat exchanger and the TE module can be used to minimize the amount of material in the heat exchanger and the pumping power required for forced convection liquid cooling. Changing the amount of solar concentration, changes the input heat flux and this is another parameter that can be optimized in order to reduce the cost of heat exchanger (by size), the tracking requirement and the whole system. A series of design curves for different solar concentration are obtained. It is shown that the overall efficiency of the system can be more than 80% at 200x concentration which is independent of the material ZT (TE figure-of-merit). For a material with ZT_{hot}~0.9, the electrical conversion efficiency is ~10%. For advanced materials with ZT_{hot}~ 2.8, the electrical conversion efficiency could reach ~21%.

1. Introduction

1.1 Residential use of solar power

Concentrated solar radiation is used in photovoltaic systems and also in solar thermal designs with turbines or with Stirling generators, for example solar farm in Spain [1] which contains steam turbine as well as in California [2] in the U.S. Also, solar trough systems are built in even smaller vacant lands, such as [3]. Currently the cost of the solar thermal electricity generation is lower than the photovoltaic cells [4], however that is mostly effective for large size systems and it is not readily scalable for distributed power generation in residential homes. Photovoltaic systems are very scalable and they are widely used in homes. However the efficiency of the systems is ~15-20% and we don't use the 70-80% of the energy which is wasted in the form of heat. Since the silicon solar cell efficiency drops by ~1% for every 10K temperature increase [5]; it is hard to think about the designs where the temperature of the photovoltaic cell is allowed to increase, and where we could use the waste heat to provide hot water to the home in combination. As another co-generation approach, special optical filters are proposed to direct the infrared radiation to a solar thermal system and the visible spectrum to PV, namely PV/T [6]. However, because of the cost and the complexity of the optical system, this solution is rarely used.

An alternative is to consider the thermoelectric direct conversion into electricity. Solar thermoelectric systems have been analyzed [7]. There is a recent micropower demonstration by Amatya and Ram [8]. The incident solar energy flux is around 1000W/m^2. If this energy is received as heat at the hot side of thermoelectric module, the incident power is still small to obtain the advantage of thermoelectric conversion. Our previous work [9] indicated that around 1e+5 W/m^2 is preferable for the heat input as this minimizes the amount of the thermoelectric material and the heat exchanger (heat sink). Therefore, the concentrated solar radiation will match well with the sweet spot of thermoelectric. However, still the energy conversion efficiency is low compared to e.g. Stirling engines.

The wasted heat from above energy conversion could be used for hot water supply in the residence application. Both electricity and hot water are essential for the human life and, typically, the hot water is produced by electricity or by burning a fossil fuel such as natural gas. Residential energy consumption is around 11.9% of whole energy use in the United States [10]. Therefore, the potential of such co-generation system to reduce the CO_2 emissions could be substantial. In this report, the optimum design, energy conversion efficiency and the material cost of such a system are investigated with analytic modeling. The model is based on the co-optimization of the thermoelectric module and the heat exchanger which was developed in previous work.

1.2 Proposed model

There are several key components for the proposed system. 1) Photons irradiated from Sun are concentrated by a Fresnel lens or by a parabolic/ non-imaging optics dish. In the analysis, the concentration ratio C is variable (unity or larger). 2) Concentrated Sun light is absorbed at the panel surface of the thermoelectric module, which is near black body (emissivity is assumed to 0.95 for the entire spectrum of interest). 3) A water cooling heat exchanger is directly attached to the back side of the thermoelectric module. The water inlet temperature is considered to contain wasted heat from e.g. bath tub or hot water drain for further potential heat energy recycling. So, it varies between 0°C and 60°C. The outlet temperature is fixed to 80°C since typical hot water supply in residential house is 60-80°C and we assume some heat loss from the system to supply end. The concept is illustrated in Fig. 1. The analysis is carried out assuming a tracking mechanism so that the Sun is always normal incident.

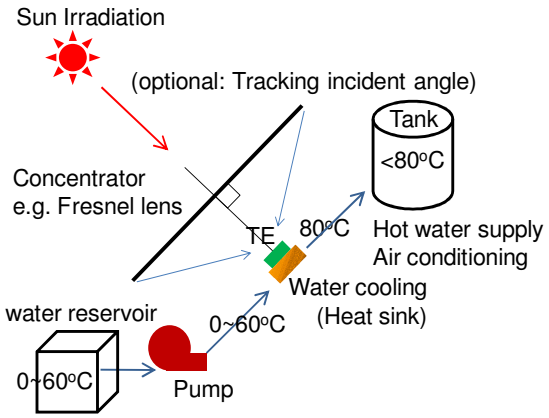

Figure 1. Residential photo-thermo-electric co-generation system

2. Metric of performance

The metric for the performance of the system can be defined by the energy conversion efficiency and the total power gain in the form of electricity or heat. These can be compared with widely used photovoltaic solar panels for electricity generation and with hot water furnaces for heat generation. The performance of the heat exchanger and the thermoelectric energy conversion depend on the sensitive heat transported to water. That means appropriate pumping power is required for the optimum operation. Therefore electric power used for water pump is deducted from the above power gain.

$$W_{ttl} = W_{TE} + \rho C_p G \Delta T - W_{pp} / \eta_e \qquad (1)$$

where, W_{TE} is electrical power output [W] from the thermoelectric module, ΔT is water temperature difference [K] between the outlet and the inlet of the heat exchanger. G is the flow rate [m^3/s], W_{pp} is the pumping power [W] and η_e is the electric to fluid power conversion efficiency. The maximum energy conversion efficiency η_{ttl} of this system is described as,

$$\eta_{ttl} = \frac{W_{ttl}}{A_{panel}} \Big/ q_B \qquad (2)$$

where, A_{panel} is the foot print area [m^2] of the concentrator panel and q_B is the heat flux [W/m^2] which can be absorbed by a black body plate on Earth.

The cost components of the system are included such as lens (e.g. Fresnel lens made of poly carbonate), thermoelectric material and heat exchanger material. The material cost is one of the key bottlenecks and it is important to identify the tradeoff between different components. Cost per unit power output [$/W] is then calculated and compared to other technologies. Mechanical fixture, piping for water flow, pump and water reservoir/tank are not considered in this analysis. They will be added in a future publication.

3. Sky temperature and heat flux

Before considering the overall thermodynamic system, the effective sky temperature T_{sky} and the heat flux at the hot side of the thermoelectric module are determined in this section following the analysis of De Vos [11]. Solar irradiation energy spectrum can be fitted by Planck law (see Eq.3). Thus, Sun temperature T_{sun} is immediately found as 5762 [K].

$$\text{Energy intensity(E)} = A \frac{E^3}{\exp\left(\frac{E}{kT}\right) - 1} \qquad (3)$$

where E [eV] is the energy of the photon. Due to the radial expansion of Sun's radiation, the energy density incident to earth is reduced by a ratio f called dilution factor, proportional to the square of the radius ratio.

$$f = \left(\frac{r_{sun}}{r_{earth}}\right)^2 = 2.15e-5 \qquad (4)$$

Considering Alberdo number of the earth α~0.3 and greenhouse factor γ~0.4, the planet temperature of earth T_p is found as,

$$T_p = \frac{(1-\alpha)^{1/4}}{(1-\gamma)^{1/4}} \frac{f^{1/4}}{\sqrt{2}} T_{sun} = 0.735 f^{1/4} T_{sun} \qquad (5)$$

Therefore, T_p=288.7 [K].

Concentration ratio C is introduced in the model as previously defined.

$$C = \frac{A_{module}}{A_{panel}} \quad (C \geq 1) \qquad (6)$$

Due to the finite temperature of Sun, maximum concentration ratio is 1/f ~4.6e+5.

Form the TE device point of view, the effective sky temperature is changed by the effect of photo magnification on the radiative heat transfer. Therefore,

$$T_{sky} = \left(CfT_{sun}{}^4 + (1-Cf)T_p{}^4\right)^{1/4} \quad (7)$$

This is the hot source temperature. Heat flux of this source is found assuming a surface emissivity of ε=0.95,

$$q_h = \varepsilon\sigma\left(CfT_{sun}{}^4 + (1-Cf)T_p{}^4 - T_h{}^4\right)/A_{module} \quad (8)$$

where, q_h [W/m^2] is heat incident to the thermoelectric module, σ is Stefan-Boltzmann constant 5.67e-8 [W/m^{2}K^4] and T_h is hot side temperature of thermoelectric module. 1st term of Eq. 8 is the radiation from Sun under concentration (note *f* is delusion factor), 2nd term is from earth and 3rd term is the radiative heat dissipation from TE module, respectively.

4. Thermoelectric module Optimization

The schematic of typical thermoelectric power generation system is shown in following figure.

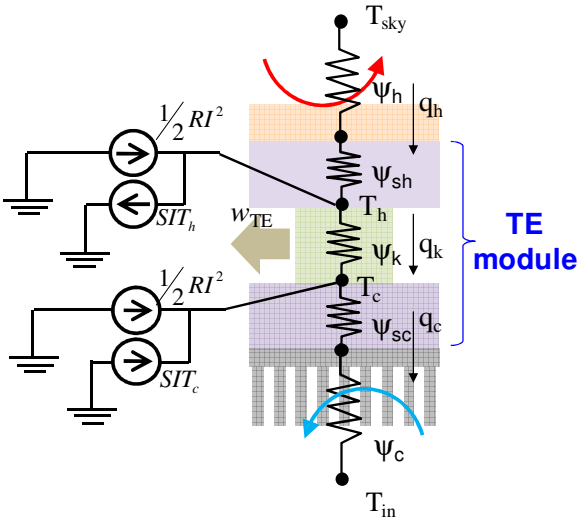

Figure 2. Equivalent thermal circuit of the TE module with heat source and heat exchanger

Following shows the energy balance at the hot side and the cold side of TE module, respectively.

$$q_h = q_k + \frac{\beta Z}{(1+m)^2 2d}\left((2m+1)T_h + T_c\right)(T_h - T_c) \quad (9)$$

$$q_c = q_k + \frac{\beta Z}{(1+m)^2 2d}\left(T_h + (2m+1)T_c\right)(T_h - T_c) \quad (10)$$

where, T_h and T_c are temperatures of hot side and cold side of TE module, respectively, β is thermal conductivity [W/mK] of thermoelement, d is leg length [m] of thermoelement, m is ratio of external load resistance [Ohm] and internal electrical resistance [Ohm], q is heat per unit area [W/m^2] with subscript h: hot side, k: thermoelement, c: cold side. The optimum TE module design for unit foot print area is established by Yazawa et al [9]. The model indicates that the optimum output is found when the thermal resistance of the module ψ_k matches to the sum of external thermal resistances Σψ multiplied by ratio *m*. This ratio *m* is common to thermal and electrical resistance match as far as $Z << 1$ and $T_{in}/T_{sky} > 0.1$ with engineering accuracy.

$$\psi_k = m\sum_{external}\psi = m\left(\psi_h + \psi_{sh} + \psi_{sc} + \psi_c\right) \quad (11)$$

$$m = \sqrt{1 + Z\frac{(T_h + T_c)}{2}} \quad (12)$$

Where, Z is the figure of merit of thermoelectric material [1/K].

For initial analysis, the impact of fractional fill factor of thermoelement inside the module is ignored. This is added in section 7 where the spreading thermal resistance related to the fractional coverage of thermoelement is considered.

The maximum output power density w_{TE} at matched electrical load resistance is given by,

$$w_{TE} = \frac{Z}{4(1+m)^2}\frac{1}{A\sum\Psi}\left(T_{sky} - T_{in}\right)^2 \quad (13)$$

and optimum leg length to yield the maximum power density is found as,

$$d = m\beta A\sum\Psi \quad (14)$$

Where, *A* is the foot print area of thermoelectric module. The smaller area induces a thinner optimum element for material saving, which will be discussed in later section. One can design the number of elements in a module considering electrical resistance match to the load resistor.

There is a specific condition to determine external thermal resistances for this system. The cold side temperature T_c is limited to the water temperature which is set to 80°C at the atmospheric pressure (103kPa). We also assume single phase heat transfer. While it is possible to use the boiling forced convection, it causes a significant change in heat transfer capability which makes the predictions difficult due to the probability and fluctuations. In addition, when there are vapor bubbles in the heat exchanger, the pressure losses are significantly larger, increasing the fluid pump power which obviously reduces the energy payback.

To find the (thermal and electrical) resistance match ratio `m`, T_h and T_c need to be determined. There is an exact solution as function of T_{sky} and T_{in}, which is the water inlet temperature.

$$(T_c - T_{in}) = \frac{\psi_c}{(\psi_c + \psi_h)} \times \frac{1}{X}\left(1 + \frac{Z}{2(1+m)^2}(T_h + (2m+1)T_c)\right)(T_h - T_c) \quad (15)$$

$$(T_{sky} - T_h) = \frac{\psi_h}{(\psi_c + \psi_h)} \times \frac{1}{X}\left(+\frac{Z}{2(1+m)^2}((2m+1)T_h + T_c)\right)(T_h - T_c) \quad (16)$$

where,

$$X = \left(1 + \frac{Z}{2(1+m)^2}((2m+1)T_h + T_c)\right)\frac{\psi_h}{\sum\psi} + \left(1 + \frac{Z}{2(1+m)^2}(T_h + (2m+1)T_c)\right)\frac{\psi_c}{\sum\psi} \quad (17)$$

If one assumes *ZT* is small, the equations are simplified as follows. Since the hot water temperature is defined to 80°C, the cold side temperature is not allowed to exceed the limited.

$$T_c = \mathrm{MIN}\left((T_{sky} + 3 * T_p)/4, 353\right) \quad (18)$$

$$T_h = (T_{sky} - T_{in})/2 + T_c \quad (19)$$

Thermal resistance of heat exchanger is now

$$\psi_c = (T_c - T_{in})/q_c = (T_c - T_{in})/(q_h - w_{TE}) \quad (20)$$

$$\psi_h = (T_{sky} - T_h)/q_h \quad (21)$$

To make fair comparison with the overall efficiency of non-concentrated technologies, such as plane photovoltaic or solar thermal systems, power gain for given panel area is calculated as,

$$W_{TE} = A_{panel} w_{TE} / C \quad (22)$$

At the next step, sensitive heat transported by convection in water flow is investigated. The amount of heat that the flow water could receive is the 100% of loss from the thermoelectric module. The heat energy raises water temperature so that,

$$Q_w = \rho C_p G(T_{out} - T_{in}) \quad (23)$$

where, ρ is density [kg/m^3] of water, C_p is specific heat [J/kgK] of water at an average temperature and G is flow rate [m^3/s] through the heat exchanger. T_{in} is inlet temperature as given. Optimization of heat exchanger is discussed in the following section and outlet temperature T_{out} is also determined by the optimum condition. But also, T_{out} is restricted up to 80°C.

5. Heat exchanger design pump power

Heat exchanger is considered to occupy the same foot print as TE module to avoid any thermal loss with spreading the heat. Direct attachment of thermoelement on the heat exchanger is a challenging topic. Here, we could consider a dielectric and good thermal conductive material for the heat exchanger e.g. AlN. Or, we could consider a dielectric layer between thermoelement and copper heat exchanger whose thermal expansion coefficient (CTE) is matched. Choosing either material, thermal resistance from the TE hot side to the heat exchanger is neglected here.

There is a significant amount of work on heat sink optimization as described e.g. in [12] [13] [14]. In this study, the model of Yazawa et al. [15] is used, but slightly modified and simplified in order to do a systematic calculation of the energy payback. Also the name 'heat exchanger' is used instead of 'heat sink' since this component transfers the heat energy to the water flow. We assume a heat exchanger where the fluid path is made of parallel channels as shown in Fig. 3. In this figure, the water flows through the channels in the direction perpendicular to the paper plane. In the previous work [9], fin thickness is precisely considered but to adapt to wider range of heat fluxes in the current study, the geometry is simplified. A single layer of parallel circular tubes channels are placed with ½ diameter gap. Therefore the thickness of the heat exchanger depends on the channel diameter.

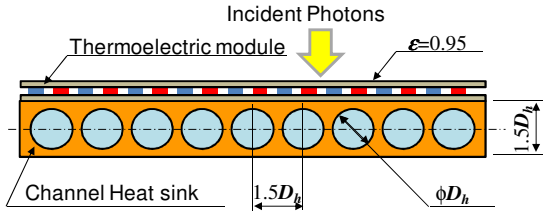

Figure 3. Heat exchanger attached to TE module

In this session, we will optimize the channel design for a given thermal resistance and pumping power in order to minimize the heat exchanger's mass. From the discussion in Ref. [15], the optimum condition can be found when the convection from the fin surface matches to that of the temperature sensitive fluid flow. This is a kind of impedance match for heat flow from the fin to the fluid reservoir. The impedance matched condition is described as,

$$U_{BASE} A_{BASE} = 1/\left(\frac{1}{2\rho C_p G} + \frac{1}{U_{fin} A_{fin}}\right) \quad (24)$$

where, the convective (fin) surface area is,

$$A_{fin} = N\pi D_h L \quad (25)$$

N is Number of channels, L is length [m] of channel. And heat transfer coefficient at convective surface is,

$$U_{fin} = \frac{Nu\beta_f}{D_h} \quad (26)$$

Nu is Nusselt number and β_f is the thermal conductivity [W/mK] of fluid (water). It is adequate to assume fully developed flow for a long aspect channel ($L>>D_h$). Thus, Nusselt number of 4.634 for circular tube [16] is applied.

The relation between convective thermal resistance and the sensitive transport thermal resistance yields the intermediate temperature T_m of the point, to where the convective heat is transferred, is half of the temperature difference as well as the half of the fluid temperature rise (T_{out}-T_{in}). From this, T_{out} is immediately found to be equal to T_c. Therefore, flow rate G is found as

$$G = \frac{(q_h - w_{TE})}{\rho C_p (T_c - T_{in})} \tag{27}$$

By substituting DL to A_{BASE} and $1/\psi_c$ instead of U_{BASE} in Eq. (24), the diameter of channel is found as:

$$D_h = \frac{\pi Nu \beta_f}{1/\psi_c} \tag{28}$$

From the geometry shown in Fig. 3, the number of channels is found as,

$$N = \frac{2D}{3D_h} - 1 \cong \frac{2D}{3D_h} \tag{29}$$

Knowing G, D_h and N, the mean flow velocity in a channel u is found as,

$$u = \frac{2G}{N\pi D_h^{\,2}} \tag{30}$$

The pressure drop ΔP_{ch} caused by friction loss in entire internal wall of the channel is determined assuming fully developed flow and the pressure loss caused by contraction/expansion is found negligible.

$$\Delta P_{ch} = \frac{48\mu L}{D_h^{\,2}} u \tag{31}$$

Finally, pumping fluid power is determined by

$$w_{pp} = G\Delta P_{ch} \tag{32}$$

Since electro-mechanical and mechanical-fluid momentum energy conversion losses exist, the efficiency needs to be considered. The overall fluid pump efficiency η_e is picked from off-the-shelf pumps and assumed to be 60%.

$$w_{e-pp} = w_{pp} / \eta_e = G\Delta P_{ch} / 0.6 \tag{33}$$

The model is based on laminar flow regime. To verify if the model predicts the pumping power correctly, Reynolds number Re can be used to see if the flow is laminar or if there is transition to turbulence. The criterion for transition to turbulent flow regime in circular tube is at a Reynolds number of around 2300. Following is the definition of circular tube based Reynolds number.

$$\mathrm{Re} = \frac{\rho u D_h}{\mu} \tag{34}$$

6. Analysis and Discussion

An example of gain and loss is shown in Fig. 4, where Z=0.001 which is equivalent to ZT=1 at high concentrated radiation temperature with the typical performance of today's state-of-the-art material. At the small concentration ratio C (less than around 3), the reason of curve distortion is that T_{out} cannot reach high values since the heat flux is not enough at the maximum TE power output. For larger C, T_{out} stays at 80°C.

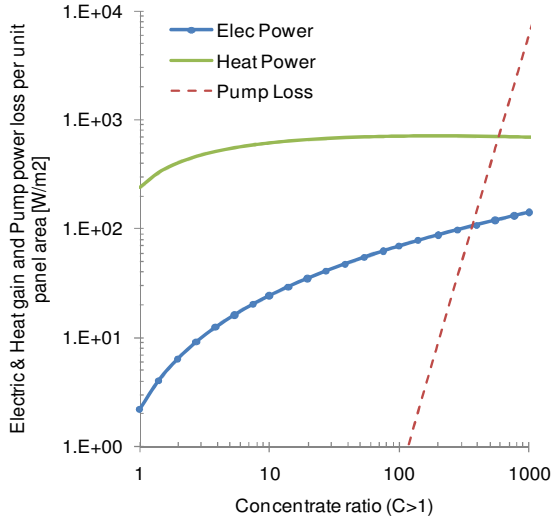

Figure 4. Gain an loss versus concentration ratio for Z=0.001, T_{in}=60°C

Some interesting trends are found here. As concentration ratio, C, goes up, thermoelectric power generation increases quickly and reaches 100W/m^2 at C=304. Since electric power is subtracted, heat power gain is gradually reduced. Heat power reaches a maximum at round C=190 and then decreases. As long as available, TE power generation goes up as concentration is increased. Another important factor is the very steep increase of the pump power which reaches the breakeven at C~680 at which there is no net electricity generation. In order to check the validity of the flow model, Re is plot in Fig. 5. Based on laminar criteria, a transition in flow regime can happen when C>200. Thus, the model could underestimate the pumping power when the solar concentration is in the range 200<C<680. The reason of low efficiency of heat energy conversion at small concentration ratio is because the heat exchanger is designed to maximize the electric power output. There will be another option to design the heat exchanger to maximize the overall energy collection in smaller concentration.

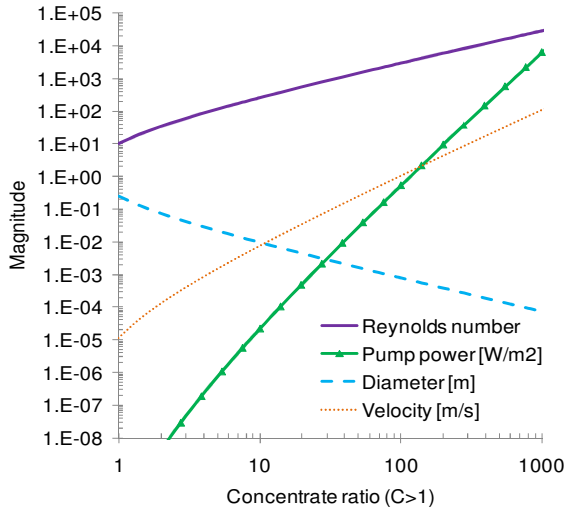

Figure 5. Fluid dynamic characteristics versus concentration ratio at Z=0.001, T_{in}=60°C

Overall efficiency is shown in Fig. 6 for Z=0.001 (representing today's high temperature thermoelectric materials) and Z=0.003 (high performance advanced materials). The overall energy conversion efficiency does not change much depending on the figure-of-merit of thermoelectric material but it does not mean these are near identical. As the electrical output is quite different and Z=0.003 gives much higher electricity generation. The ratio of water heating generated and the output electric power depends strongly on the performance of the thermoelectric material.

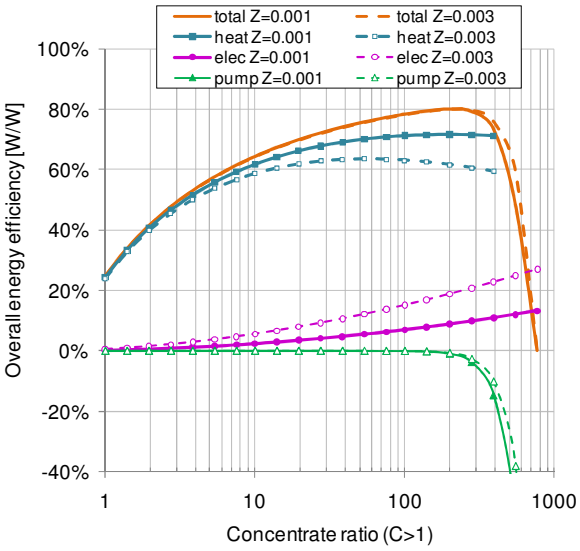

Figure 6. Efficiency of the overall co-generation system and the water heating part versus concentration ratio for Z=0.001 and 0.003

Fig. 7 is a 3D plot of overall efficiency for various water temperatures and the concentration ratios. Highest efficiency is around concentration ratio of 500~2000. The maximum efficiency reaches 80% for any inlet temperature.

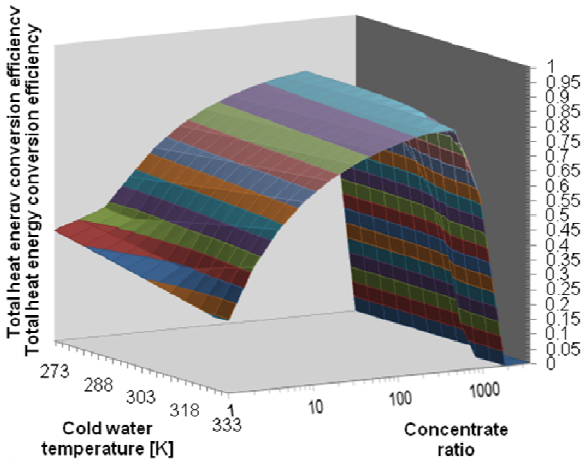

Figure 7. Total efficiency of the cogeneration system as a function of water inlet temperature and concentration ratio. Z=0.001 is assumed.

Because of steep decline of the curve over the peak versus concentration ratio, the engineering optimum could be determined at 95% of peak, where the overall energy efficiency is 78% for any inlet temperature and is at the concentration ratio of around 120 <C<250. This condition corresponds to the laminar flow limit. Therefore, 200 Suns concentration ratio can be a suggested condition to obtain near optimum energy efficiency 78%.

7. Cost consideration

In this section the cost of the system is investigated. Different solar concentration technologies and the scalability challenge of lens are not considered. To produce a simple example, Fresnel lens made of polycarbonate is considered. The thickness of the lens depends on the panel size. Here we consider a fixed lens cost per unit area 1m^2. The cost of the rigid mechanical frame and the tracker is not included and it will be discussed in future publications. The cost of the lens panel is based on material price in the range of $3/kg. Heat exchanger cost is based on copper price $7.3/kg. Thermoelectric material that needs to be considered depends on the temperature range which is related to the concentration ratio. As a simple estimation, the thermoelectric material cost is based on Bi_2Te_3 that is approximately $500/kg. The substrate material (e.g. AlN) for TE module is assumed $100/kg. The footprint area of TE module and heat exchanger linearly shrink as concentration ratio increases.

As reported [7], we consider a thermoelement with Z between 0.001~0.003 [1/K], thermal conductivity of 1.5 [W/mK] and a thickness of 2e-4 [m] for TE module substrate. In this section we add an additional degree of freedom where the thermoelectric legs could cover a fraction, F, of the area of the TE hot and gold plates. F can affect the optimum leg thickness and the amount of TE material in the module. There is an additional spreading thermal resistance at small fractional area

coverage. In ref. [7] it was shown that the output power degradation due to fractional coverage in range of 0.01~1 is negligible. Fig. 8 shows the overall material cost per total output power of the cogeneration system. The fractional area coverage of thermoelement yields great impact in terms of cost performance at low solar concentrations. However, when the concentration ratio is bigger than 100, the energy cost converges to almost a single number around 0.1 $/W. We will see later that this is dominated by the cost of the optical system. The steep increase in cost observed at around concentration ratio of 500 is due to the rapid increase of the cooling need which requires significant pumping power. The difference due to material's Z parameter is small if we could prepare the same Z for different temperature ranges. As we saw in Fig. 6, Z affects strongly the ratio of output electrical power versus thermal energy in the hot water while concentration ratio is larger.

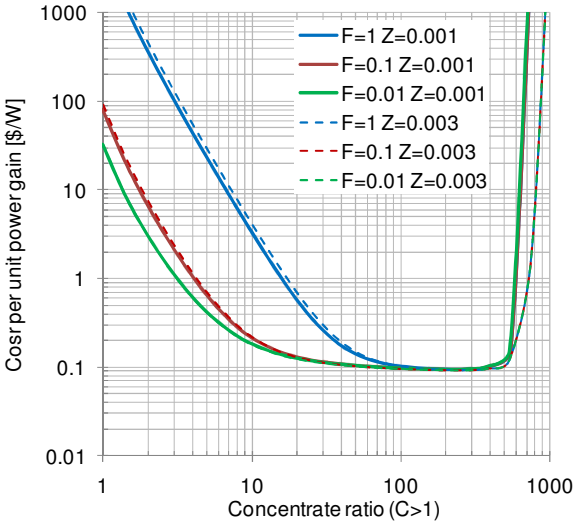

Figure 8. Cost per total output power [$/W] versus concentration ratio for different TE module fill factors. T_{in}=60°C, Z=0.001 and 0.003 are assumed.

Fig. 9 separates the costs of electric energy output and heat output. This should help for the comparison with the existing solar electric and solar thermal systems. One should remember that this is a co-generation scheme and that electrical and thermal energies are co-produced. Considering the market price of conventional photovoltaic panel with poly-silicon is in range of 2.5-3.0 $/W, the thermoelectric co-generation system could be a competitive renewable energy solution. The cost contributions for different components are shown in Fig.10 and Fig. 11 in relative. At C~200, the optics (Fresnel lens panel) dominates the cost. This implies that there are opportunities to further reduce the cost using different concentration technologies.

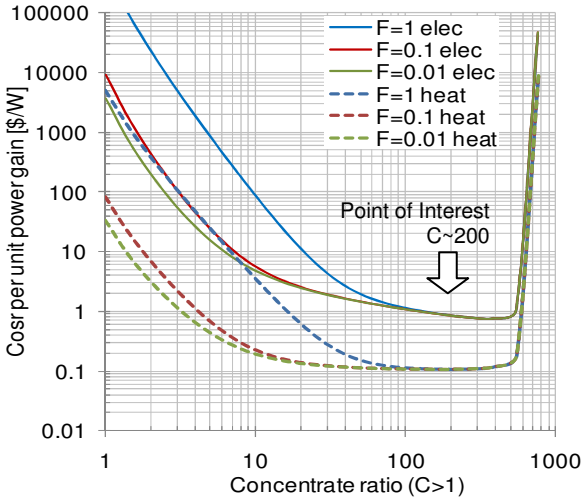

Figure 9. Cost per power output [$/W] for both hot water and electricity versus concentration ratio for different TE module fill factors. T_{in}=60°C and Z=0.001 are assumed.

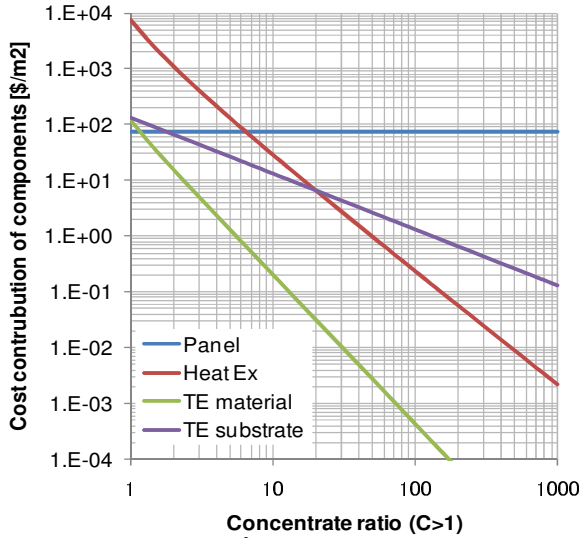

Figure 10. Cost [$/m^2] contribution of components assuming F=0.01

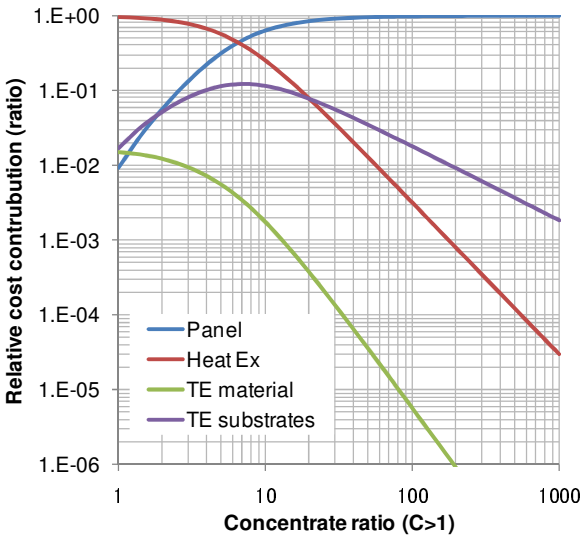

Figure 11. Relative cost contribution of components assuming F=0.01

Table 1 shows the cost of energy conversion systems of different sizes based on the projected data of 2010 from DOE report in 1997 [17]. Even though this report is relatively old, the current market price of photovoltaic panel is quite similar.

Table 1 Cost of various solar energy conversion technologies from DOE report ref. [17]

		Scale [MW]	Cost [$/W]
Photo voltaic	Residential	0.003	2.98
	Thinfilm Flat	16.000	1.50
	Concentrator	17.000	1.55
Solar thermal	Through	320.000	3.00
	Tower	200.000	2.61
	Dish	30.000	1.69

8. Conclusions

In this paper, we proposed a system for co-generation of electricity and heating for hot water which are both essential for residential applications. This is based on solar concentrator and thermoelectric module with hot water microchannel heat exchanger. Optimum design of the thermoelectric system is calculated and plugged into the thermodynamic system. Most of the energy not converted to electricity by the TE module is used to warm up the water. The benefit of this combination is that thermoelectric material can be chosen in a wide range of temperatures so that it is optimized for various concentration ratios. Heat exchanges are also optimally designed. The electrical output power is maximized by reducing the needed water pump power for each concentration ratio.

The results show quite high overall energy efficiencies with a peak around 80%. The peak does not depend on the figure-of-merit of TE element but the energy gain ratio Electricity/Hot water is changed significantly as function of *ZT*. Higher concentration ratios tend to yield better output power. However, due to the very steep increase of pump power penalty, the engineering maximum can be found at around 200 Suns. Current analysis takes into account material cost for different components of the co-generation system. This is important to study tradeoffs and the cost limits. Future work will focus on the impact of the tracking, other components of the system and the role of the parasitic electrical and thermal resistances in the TE module.

9. Acknowledgement

This work was supported by Center for Energy Efficient Materials funded by the Office of Basic Energy Sciences of the US Department of Energy. Authors also thank to Mr. Kahlil Morse, who helped with the cost information.

10. References

[1] K. Schneider, 1981, “EURELIOS. The 1 MW solar power plant of the European Communities”, *Neue Deliwa-Z. Journal* Vol. 32:2, pp39-40

[2] C. A. Ogaja, 2010, "Crustal Dynamic in California: Implications for Large-Scale CSP Tower Systems", *Proceedings of SOLAR 2010 Conference*, ASES

[3] H. Price et al. 2002, 'Advance in Parabolic Trough Solar Power Technology", *J. Sol. Energy Eng.*, Volume 124, Issue 2, pp109-116

[4] National Renewable Energy Laboratory, 2010, “Energy Technology Cost and Performance Data”, http://www.nrel.gov/analysis/tech_costs.html

[5] G. A. Landis, 2005, “High-Temperature Solar Cell Development”, *NASA report* NASA/CP—2005-213431, pp 241-247

[6] H.A. Zondag, 2008, "Flat-plate PV-Thermal collectors and systems: A review", *Renewable and Sustainable Energy Reviews*, Volume 12, Issue 4, pp891-959

[7] J. Baxter et al., 2009, “Nanoscale design to enable the revolution in renewable energy”, *Energy & Environmental Science 2009*, Vol.2, pp559-588

[8] R Amatya and R. J Ram, 2010, “Solar Thermoelectric Generator for Micropower Applications”, *Journal of Electronic Materials*, Vol. 39, No. 9, pp1735-1740

[9] K. Yazawa and A. Shakouri, 2010, “Energy Payback Optimization of Thermoelectric Power Generator Systems”, *Proceedings of ASME IMECE2010*, IMECE2010-37957

[10] Lawrence Livermore National Laboratory, 2010, “Estimated U.S. Energy Use in 2009”, https://publicaffairs.llnl.gov/news/energy/energy.html

[11] A. De Vos, 1992, “Endoreversible Thermodynamics of Solar Energy Conversion”, Oxford press

[12] Y. Murakami, Y. et al., 2001, “Parametric Optimization of Multichanneled Heat Sinks for VLSI Chip Cooling”, *IEEE Transaction on Components and Packaging Technologies*, Vol. 24, No. 1, pp2-9

[13] P. Teertstra et al., 1999, “Analytic Modeling of Forced Convection in Slotted Plate Fin Heat Sinks”, *Proceedings of 1999 ASME International Mechanical Engineering Congress and Exposition,* HTD-Vol. 364-1, Vol.1, pp3-11

[14] M. Iyengar et al., 2003, “Least-Energy Optimization of Air-Cooled Heat Sinks for Sustainable Development”, *IEEE CPT Transactions*, Vol. 26, No.1, pp16-25

[15] K. Yazawa et al. 2003, “Thermofluid Design of Energy Efficient and Compact Heat”, *Proceedings of 2003 International Electronic Packaging Technical Conference and Exhibition,* IPACK2003-35242

[16] eds. W. R. Rohsenow et al., 1998, “Forced Convection, Internal Flow Ducts”, *Handbook of Heat Transfer third edition*, pp5.7

[17] E.A. DeMeo et al, 1997, "Renewable Energy Technology Characterizations", *DOE Topical Report*, TR-109496, http://www1.eere.energy.gov/ba/pba/tech_characterizations.html